34th Annual International Conference of the IEEE EMBS
San Diego, California USA, 28 August - 1 September, 2012

A Correlated Microwave-Acoustic Imaging Method for Early-Stage Cancer Detection

Fei Gao, Yuanjin Zheng, *Member, IEEE*

***Abstract*— Microwave-based imaging technique shows large potential in detecting early-stage cancer due to significant dielectric contrast between tumor and surrounding healthy tissue. In this paper, we present a new way named Correlated Microwave-Acoustic Imaging (CMAI) of combining two microwave-based imaging modalities: confocal microwave imaging(CMI) by detecting scattered microwave signal, and microwave-induced thermo-acoustic imaging (TAI) by detecting induced acoustic signal arising from microwave energy absorption and thermal expansion. Necessity of combining CMI and TAI is analyzed theoretically, and by applying simple algorithm to CMI and TAI separately, we propose an image correlation approach merging CMI and TAI together to achieve better performance in terms of resolution and contrast. Preliminary numerical simulation shows promising results in case of low contrast and large variation scenarios. A UWB transmitter is designed and tested for future complete system implementation. This preliminary study inspires us to develop a new medical imaging modality CMAI to achieve real-time, high resolution and high contrast simultaneously.**

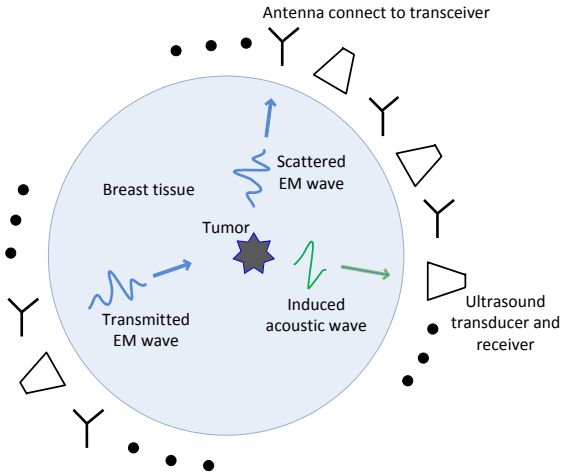

Figure 1. System setup for merging CMI and TAI

I. Introduction

Early detection is very important for effective treatment of cancer [1]. Previous studies have shown that at microwave frequencies, the dielectric properties of cancerous tumor is much different from the healthy tissue, which is the basis of microwave-based imaging method for cancer diagnosis [2]-[3]. By detecting the large dielectric contrast, various microwave-based imaging modalities have been proposed, among which, confocal microwave imaging (CMI) and microwave-induced thermo-acoustic imaging (TAI) are attracting significant attentions in recent years. Compared with microwave tomography that is solving a scattering inverse problem to reconstruct the dielectric distribution, CMI is using antenna array to transmit UWB pulse alternately and receive the scattered signals at different locations. Tumor could be detected from these received signals by various beamforming techniques [4]-[5]. Interestingly, apart from the scattering caused by dielectric difference of tumor, energy absorption also exists when microwave is propagating in the tissue. Due to higher water content in tumor, it absorbs more microwave energy than surrounding healthy tissue. Following tissue heating, thermo-acoustic expansion and tissue vibration, acoustic signals are generated and eradiating to the surface of the body, which are detected by the ultrasound transducers placed around the objective sample [6]-[7]. The received acoustic signals carrying the information of tissue EM absorption, could also be used for tumor detection. Through detecting the scattered microwave signals and induced acoustic signals for imaging simultaneously, we expect to correlate these two images to improve resolution and contrast significantly.

In this paper, we propose a new image correlation method named Correlated Microwave-Acoustic Imaging (CMAI) by merging CMI and TAI to achieve higher contrast, resolution rather than any one of them. A UWB transmitter is also designed for the whole system implementation in the future work.

II. System Configuration

A. System Setup

System configuration is shown in Figure 1, objective sample is modeled as a circle filled with heterogeneous healthy human tissue, where a tumor with different dielectric property is embedded [8]. Microwave antennas are placed around to transmit UWB signals and receive scattered signals. Ultrasound transducers are also placed around for acoustic signals detection. This setup allows collecting both microwave and acoustic signals for image reconstruction.

B. Confocal Microwave Imaging

By solving the Maxwell's equations in heterogeneous medium, the scattered electric field $Escat$ could be derived as [9]:

This work was supported by National Medical Research Council of Singapore under Grant MH95:03/1-42.

Fei Gao and Yuanjin Zheng are with the School of Electrical and Electronics Engineering, Nanyang Technological University, Singapore, 639798. (phone: 65-94494530; e-mail: fgao1@e.ntu.edu.sg; yjzheng @ntu.edu.sg).

$$Escat = \omega^2\mu(1+\frac{\nabla\nabla\cdot}{k_b^2})\int_V E(r')g(r,r')[\varepsilon^*(r')-\varepsilon_b^*]dV' \quad (1)$$

where ω and μ are the angular frequency and permeability of the medium, $\varepsilon^*(r')$ and ε_b^* are the permittivity of tumor and surrounding normal tissue, $k_b = \omega\sqrt{\mu\varepsilon_b^*}$ and $g(r,r') = e^{-jk_b|r-r'|}/4\pi|r-r'|$ is the Green's function. From above equation we see that strong scattering occurs at the interface of permittivity mismatch. Instead of solving the inverse problem of the equation for dielectric distribution mapping, CMI is to directly process the scattered signals for tumor detection. Signal pre-processing is illustrated in Fig 2, followed by conventional delay-and-sum algorithm for image reconstruction.

C. Microwave-induced Thermoacoustic Imaging

When EM wave is propagating in the lossy human tissue, energy absorption occurs leading to transient temperature rising and thermal expansion. Induced acoustic wave goes outwards to the surface of the body following the wave equation [7]:

$$\nabla^2 p(r,t) - \frac{1}{c^2}\frac{\partial^2}{\partial t^2}p(r,t) = -\frac{\beta}{C_P}\frac{\partial}{\partial t}H(r',t') \quad (2)$$

where p(r,t) is the acoustic pressure signal, c is acoustic velocity in tissue, β is thermal expansion coefficient, Cp is the specific heat, $t' = (|r-r'|/c)$, and the heating function $H(r',t') = A(r')I(t')$, where A(r) is absorption distribution and I(t) is the temporal illumination function. Solving this equation gives:

$$p(r,t) = \frac{\beta}{4\pi C_P}\iiint \frac{d^3r'}{|r-r'|}A(r')\frac{dI(t')}{dt'} \quad (3)$$

It is easy to see that the induced acoustic signal is propotional to the absorption distribution. Modified backprojection method is used for image reconstruction, revealing the absorption property of human tissue for tumor detection. Signal flow is shown in Fig 2.

III. Correlated Microwave-Acoustic Imaging

According to the analysis before, both CMI and TAI are showing the dielectric properties of human tissue, i.e., the relative permittivity and conductivity. Thus we expect that combining of this two methods in some way will result in better performance. A correlated microwave-acoustic imaging (CMAI) method is proposed to strengthen the tumor detection and suppress the clutters in both images, shown in Figure 2. Numerical simulation in part V shows significant performance improvement.

A. Analysis

Although the imaging basis of both CMI and TAI are dielectric difference of tumor and healthy human tissue, they are acquired in totally different ways: scattered EM wave and induced acoustic wave. Due to the difference of their energy existence (EM wave and acoustic wave), they propagate in separated channels and suffer respective noise sources. Therefore, for the images of CMI and TAI, it is expected that they are correlated at the tumor location (strong scattering and absorption), and uncorrelated at other locations (different forms of noise source). In addition, CMI has good contrast but poor resolution; while TAI can achieve good resolution and normal contrast. Hence, we proposed CMAI method to merge CMI and TAI together for both high resolution and high contrast.

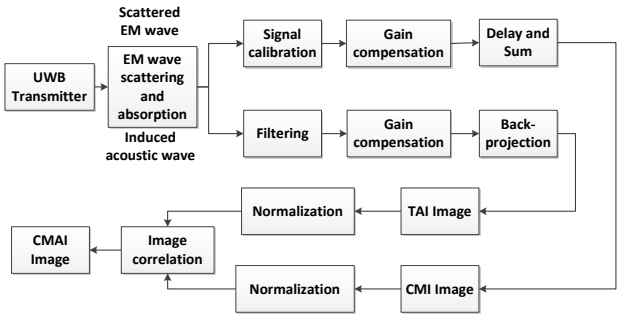

Figure 2. Signal processing for CMI and TAI

B. Proposed CMAI method

CMI and TAI images are obtained using the simple algorithm mentioned above. Due to different reconstruction ways of CMI and TAI, scaling procedure should be applied for both images to have same scale range and then shift by their mean values, as illustrated in (4) and (5). After scaling to the same range, CMI and TAI images are correlated as in (6):

$$\text{CMI image: } A(i,j) = \frac{A(i,j) - \text{mean}[A(i,j)]}{\max[A(i,j)]} \quad (4)$$

$$\text{TAI image: } B(i,j) = \frac{B(i,j) - \text{mean}[B(i,j)]}{\max[B(i,j)]} \quad (5)$$

$$\text{CMAI image: } C(i,j) = \frac{\sum_{m=i-l}^{i+l}\sum_{n=j-s}^{j+s}A(m,n)B(m,n)}{(2l+1)(2s+1)} \quad (6)$$

where the correlated image C(i, j) is obtained by multiplying the corresponding elements of CMI and TAI images in a rectangular area of size $(2l+1)x(2s+1)$, adding together, and then averaging. By this way, at the tumor location, the elements of A and B are highly correlated, where multiplication and summation leads to significantly amplification and sharpening of the tumor. While for other locations, due to different noise sources and clutters, the elements of A and B are uncorrelated, i.e., both positive and negative values exist, their multiplication and then summation tend to be zero. Therefore, through this kind of image correlation, the tumor is supposed to be enhanced and clutters to be suppressed effectively

IV. UWB Transmitter Design

An on-off LC oscillator based pulse generator with high peak power and efficiency is shown in Figure 3, which is designed and tested based on the previous work [10]. It includes a digital pulse generator, a LC VCO and a driver amplifier. On-Off Keying (OOK) with RZ input data is adopted to simplify the circuit. From simulation, the pulse generator is capable of generating nano-second pulse

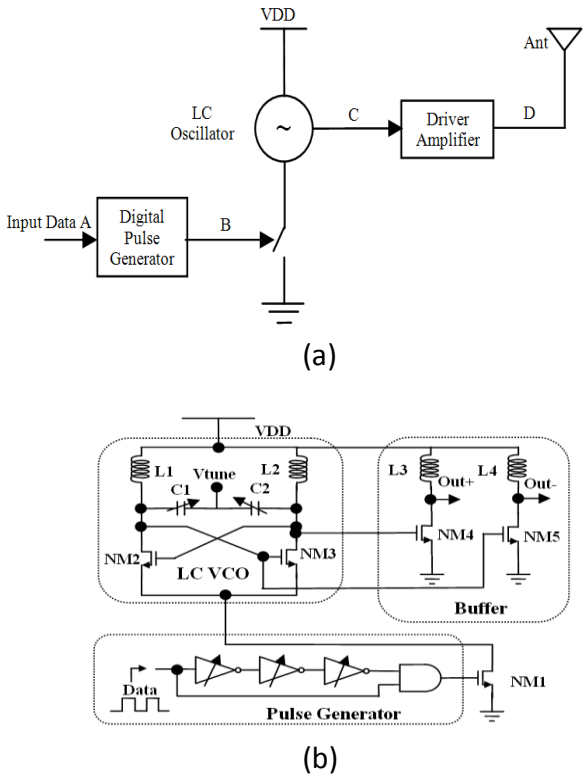

Figure 3. (a) UWB transmitter architechture, (b) Circuit schematic.

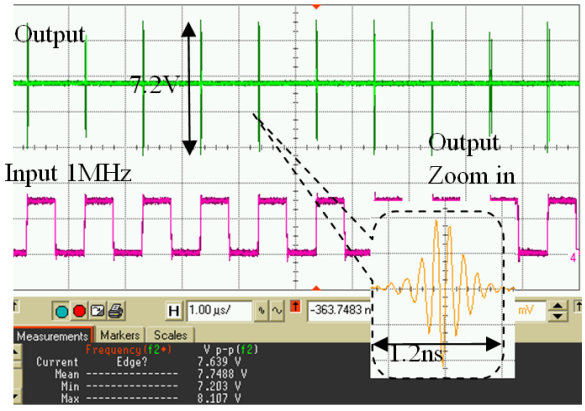

Figure 4. Measured time-domain UWB pulse.

according to the rising edge of the RZ input data, and the total setup time can be controlled to be within 255ps.

The transmitter chip is realized in Chartered's 0.18µm process and occupies an area of 0.8mm x 0.6mm(core circuit). With 1 Mbps baseband input data, the circuit can generates a pulse with 2GHz bandwidth(-20dB). Figure 4 shows the output pulse with 1.2ns width and peak swing of 7.2V, which is high enough for future imaging prototyping, and within the maximum permissible exposure (MPE) of radio frequency EM fields (3kHz to 300 GHz).

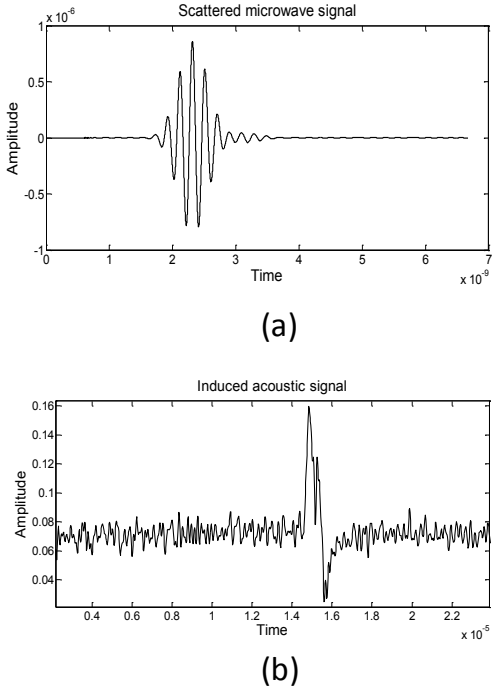

Figure 5. Waveform of (a) scttered microwave signal and (b) induced acoustic signal.

V. Numerical Simulation

Finite-difference time-domain (FDTD) method is used for the simulation of EM wave scattering and acoustic wave propagation [11]. A simulated UWB signal, representing similar waveform with measured transmitter's output signal, is transmitted into human tissue model. Scattered microwave and induced acoustic wave shown in Figure 5(a) and (b) are collected by microwave receivers and ultrasound transducers placed around objective sample at the same time.

The field of imaging is modeled as a 2D planar region (141x201) with 0.4mm resolution, modeling healthy human tissue. Tumor is embedded as a circle with 1.6mm radius. We set two scenarios of low contrast and large variation to test the performance of our proposed correlation method. Dielectric parameters are specified in Table II.

VI. Results and Discussion

In table I, three cases for low contrast scenarios and three cases for large variations scenarios are simulated, where $\varepsilon_r/\varepsilon_b$ specifies the dielectric contrast ratio of tumor and surrounding healthy tissue, and ε_b variation is modeling the heterogeneous properties of human tissue. Signal to clutter ratio (*S/C*) for these 6 cases are shown in Figure 6. The *S/C* is deteriorating when dielectric contrast is decreasing and dielectric variation is increasing. In either case, the CMAI outperforms the CMI and the TAI with 2.5dB and 0.5dB improvement respectively.

An extreme case by giving contrast as low as 1.4:1 and variation as large as 9% is tested using the three approaches. Simulation result is shown in Figure 7, it is seen that for only

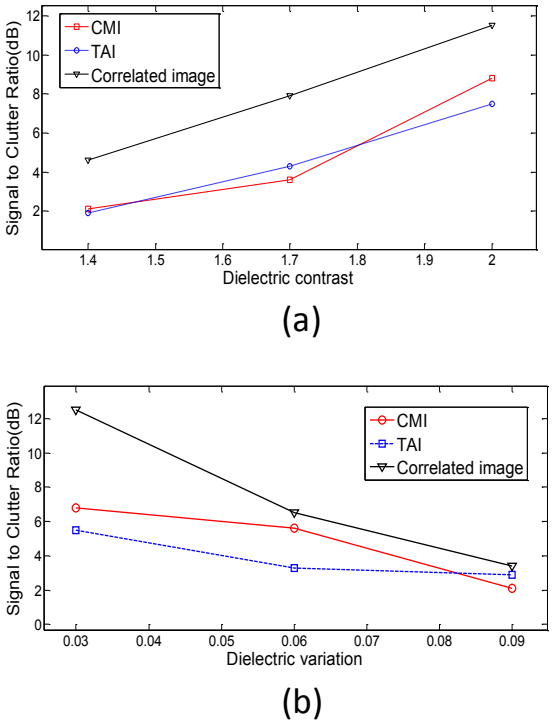

Figure 6. Signal to Clutter ratio is decreasing with (a) lower contrast and (b) larger variation.

TABLE I. DIELECTIRC PROPERTIES OF 6 CASES

Table Head	**Dielectric properties**					
	Low contrast scenario			***High variation scenario***		
$\varepsilon_r/\varepsilon_b$	2.0	1.7	1.4	2.0		
ε_b variation	3%			3%	6%	9%

CMI or TAI reconstructed image, the tumor cannot be identified clearly due to strong clutter in Fig. 7(b), which is the result of multiple scattering of microwave in human tissue, and noise caused by heterogeneous tissue heating in Fig. 7(c) . However, by the proposed CMAI method (Fig. 7(d)), the tumor is detected clearly by strengthening the correlated tumor part and suppressing other uncorrelated clutter parts.

VII. CONCLUSION

In this paper, we propose a new imaging correlation approach CMAI to merge CMI and TAI . Avoiding complicated reconstruction algorithms of CMI and TAI proposed before, we apply simple reconstruction algorithm and the proposed CMAI method obtains much better performance in terms of resolution, contrast and speed.

A UWB transmitter is designed specifically for the UWB signal generation with high peak voltage and efficiency, which will be embedded in the whole imaging system for experimental verification in our future work. Considering its high potential of integrated circuit integration, we expect to develop the CMAI into a portable microwave-based imaging device for early-stage cancer monitoring.

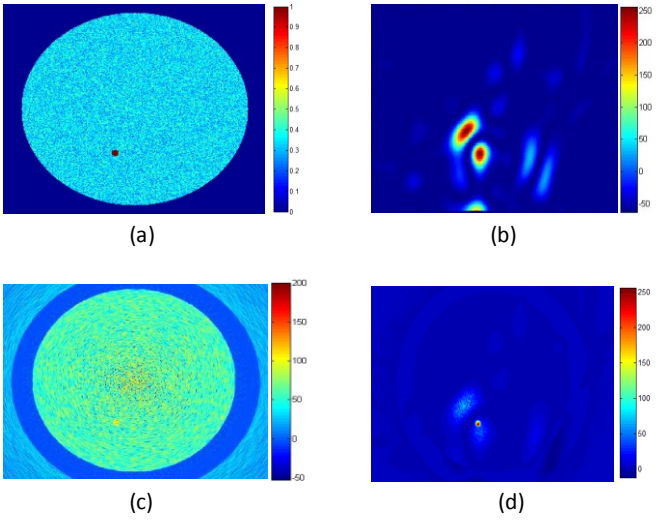

Figure 7. (a) Dielectric distribution, and reconstructed images by (b) Confocal microwave imaging, (c) Microwave-induced thermoacoustic imaging and (d) proposed correlated imaging.

REFERENCES

[1] E. C. Fear, P. M. Meaney, and M. A. Stuchly, "Microwaves for breast cancer detection," *IEEE Potentials*, vol. 22, no. 1, pp. 12–18, Feb./Mar. 2003.

[2] S. Gabriel, R. W. Lau, and C. Gabriel, "The dielectric properties of biological tissues: III. Parametric models for the dielectric spectrum of tissues," *Phys. Med. Biol.*, vol. 41, pp. 2271–2293, Nov. 1996.

[3] M. Lazebnik, L. McCartney, D. Popovic, C. B. Watkins, M. J. Lindstrom, J. Harter, S. Sewall, A. Magliocco, J. H. Booske, M. Okoniewski, and S. C. Hagness, "A large-scale study of the ultrawideband microwave dielectric properties of normal breast tissue obtained from reduction surgeries," *Phys. Med. Biol.*, vol. 52, pp. 2637–2656, 2007.

[4] E. J. Bond, X. Li, S. C. Hagness, and B. D. Van Veen, "Microwave imaging via space-time beamforming for early detection of breast cancer," *IEEE Trans. Antennas Propagat.*, vol. 51, no. 8, pp. 1690–1705, Aug. 2003.

[5] Y. Xie, B. Guo, L. Xu, J. Li, and P. Stoica, "Multi-static adaptive microwave imaging for early breast cancer detection," *IEEE Trans. Biomed. Eng.*, vol. 53, no. 8, pp. 1647–1657, Aug. 2006.

[6] R. A. Kruger, K. K. Kopecky, A. M. Aisen, D. R. Reinecke, G. A.Kruger, and W. L. Kiser, "Thermoacoustic CT with radio waves: A medical imaging paradigm," *Radiology*, vol. 211, pp. 275–278, Apr. 1999.

[7] M. Xu, Y. Xu, and L. V. Wang, "Time-domain reconstruction algorithms and numerical simulations for thermoacoustic tomography in various geometries," *IEEE Trans. Biomed. Eng.*, vol. 50, no. 9, pp. 1086–1099, Sep. 2003.

[8] E. Kirshin,B. Oreshkin, K. G. Zhu, M. Popovic, M. Coates, "Fusing microwave radar and microwave-induced thermoacoustics for breast cancer detection, " in *Biomedical Imaging: From Nano to Macro, 2011 IEEE International Symposium on*, 2011, pp. 113-116.

[9] Ali, M.A. and M. Moghaddam, "3D Nonlinear Super-Resolution Microwave Inversion Technique Using Time-Domain Data," *IEEE Trans. Antennas Propagat.*, vol. 58, no. 7, pp. 2327–2336, Jul. 2010.

[10] S. Diao, Y. Zheng, "An ultra low power and high efficiency UWB transmitter for WPAN applications", *IEEE ESSCIRC*, Sept. 2008, pp. 334-337.

[11] A. Taflove and S. C. Hagness, Computational Electrodynamics: The Finite- Difference Time-Domain Method, 2nd ed. Boston, MA: Artech House, 2000.